31st Congress of the International Council of the Aeronautical Sciences

Belo Horizonte, Brazil; September 09-14, 2018

ARAMID-FIBER REINFORCED ELASTOMERS AS FUTURE AIRCRAFT ACTUATORS—A PROOF-OF-CONCEPT INVESTIGATION

Mikko Kanerva* , **Minna Poikelispää*** , **Paulo Antunes****
*Tampere University of Technology, Laboratory of Materials Science,
P.O. Box 589, FIN-33101 Tampere, Finland
**I3N & Aveiro Physics Department and Instituto de Telecomunicações,
Campus Universitário de Santiago, P-3810-193 Aveiro, Portugal

Keywords: *Actuator, Elastomer, Composite, Conceptual design, Finite element analysis*

Abstract

In this investigation, we focus on elastomer actuators with aramid-fiber reinforcement. Proper reinforcement of elastomer actuators improves the efficiency of the actuator and is used to adjust anisotropy mainly controlling actuators' bending response. Experimental and finite element simulation results are presented in the report.

1 Introduction

The revolutionary era of various kinds of unmanned aerial vehicles (UAVs) has begun and the performance limits of traditional aircraft are being exceeded. For example, due to the lack of pilot onboard, the flight performance in terms of accelerations can be extended far beyond human strength. Also, depending on the authorized flight zone, the redundancy as well as the reliability of the structures and systems can be re-considered. For the UAVs smallest in size, many new technologies have been developed and applied on the system level. To make UAVs lightweight, heavy-duty systems such as hydraulics are typically omitted.

Soft actuators have been used rather extensively within robotics, where different modern autonomous systems must be adaptable. The adaptability means that different robot arms must not harm or damage surfaces that they might hit. For example, the McKibben actuators are already well-known and have several commercialized applications. The most potential soft actuators are fibre-reinforced to control the material behaviour of the actuator body. [1] [2]

For aeronautics, fibre-reinforced elastomer actuators could be the future option as a lightweight actuator with exceptional damping characteristics. We have recently studied the design of reinforcement of different elastomer actuators to maximize the force and displacement output in the bending mode [3]. These features of a tubular actuator are affected by the elastomer selection (i.e., hardness, Young's modulus, and compressibility), reinforcement type, reinforcement design (i.e., location and size of axial stiffener, number of fiber turns over the tube per length, number or fiber layers), and the applied pressure.

Due to the multiplicity of the factors affecting the actuator performance, numerical simulations are necessary to be carried out. Elastomers present the classical challenges of defining the material model for a hyper-elastic, incompressible media to be computed by a finite element code. Already producing high-quality test data for Poisson's ratio and force-strain curves is challenging.

In this study, we present a survey of the different actuator technologies available for flying

vehicles of any size. A summary of the literature research and an experimental work carried at Tampere University of Technology are given in the first part. In the second part, we focus on the experimental procedures for acquiring data for numerical material models for finite element methods (FEM). In the third part, we focus on the simulation of different reinforced elastomer actuators to screen the capabilities of actuators based on natural rubber and aramid-fiber.

2 Current actuator technologies

2.1 Traditional actuators

Traditional actuators for flap, aileron or rudder actuation in aircraft are carbon steel and high-strength steel based heavy-duty structures with servo hydraulic power input. These traditional actuators typically have a significant force output compared to their mass (weight efficiency). For example, mechanical input type actuators weigh 2.3...27 kg covering a rated force range of 4.4...178 kN [4], which leads to a weight efficiency range of 1900...6600 N/kg.

An electro-mechanical servo actuator is a typical solution for UAVs. For the tiniest UAVs, or model planes, the actuators are extremely simple and small. The lightest actuators weigh only $\approx$1 g and can exert a 0.054 N-actuation force (presuming a 4.7 mm moment arm) [5], giving approximately 0.05 N/g (50 N/kg) weight efficiency. Both translative and rotational electro-mechanical actuation exist.

2.2 Soft actuators

Soft actuators cover rather a wide range of technologies. Typically they are understood as shape memory alloy (SMA) based systems, electroactive polymers, and pneumatic actuators. A vast amount of research has been subjected to SMAs. For aeronautical applications, SMAs incur problems such as slow actuation speed, hysteresis, and coupling with the thermoelastic environment (of aircraft). Electroactive polymers (EAPs) divide into ionic EAPs and electronic EAPs. Again, ionic EAPs perform very slow actuation and incur hysteresis. Electronic EAPs are based on dielectric elastomers and have true potential in airborne vehicles. Actually, foldable electronic EAPs have been constructed as microair vehicle actuators and can create forces up to 0.102 N and weigh 14.4 g—giving weight efficiency of 7.1 N/kg [6].

Pneumatic soft actuators include air bellows, pneumatic muscles, and fully elastomeric multi-cell actuators. Air bellows are very simple in their structure, can be used for high-frequency dynamic actuation, and they can be relatively light-weight [7]. The downside of air bellows is that their force output is directly proportional to the actuation distance—the further the bellow actuates, the less is the actuation force [8].

McKibben actuators have been used for decades and commercial pneumatic actuators are available. The weigh efficiency of typical McKibben actuators is of the order of that of air bellows and they have merely been developed for uniaxial actuation. Specialized soft pneumatic actuators have been developed, e.g. for twisting motion [10]. Pneunets' actuators represent the multi-cell actuators. Pneunets actuators by Soft Robotics Toolkit are advanced soft actuators as regards the geometry and the respective actuation force and movement [9]. Complex sets of channels and multi-material cells makes it possible to create systems that mimic nature and are optimized concerning speed, force and weight.

3 Experiments

3.1 Materials

Pneumatic actuators are a potential concept for actuators of flying vehicles and they can be extensively modified. Therefore, we chose to study the applicability of reinforced pneumatic elastomer actuators in detail. We targeted to bending actuators, which can create moments and work as actuators without additional mechanisms in theory. Two different elastomeric materials were selected for the experiments:

- natural rubber (NR);

- polydimethylosiloxane (PDMS) in ST-EZ-60-001 tube form (provided by Etra & Silikon-Technik Siltec GmbH).

Natural rubber, NR, was selected because its composition and final form can be easily adjusted. NR compound was mixed in-house by adding 45 phr N-234 carbon black as well as other ingredients, such as curatives (sulphur, N-Cyclohexyl-2-Benzothiazolesulfenamide, CBS), zinc oxide, stearic acid, antioxidants (N-(1,3-dimethylbutyl)-N'-phenyl-1,4-Benzenediamine, 2,2,4-trimethyl-1,2-dihydroquinoline) and plasticizer (distillate aromatic extract oil). The mixing was performed by using a GK 1.5 E intermeshing mixer (Krupp Elastomertechnik). CBS and sulphur were mixed by using an open two-roll mill.

3.2 Specimen preparation

To create anisotropic elastomer actuators and control the bending upon loading, reinforcement was applied axially on one side of each tubular actuator body. Three different stiffener types were considered: polyamide (PA) fabric, pressure sensitive tape, and aramid fibre (Technora T-240, Teijin). For all actuators, radial expansion of the actuator body was controlled by manually bundle-winding aramid fibre around the elastomer tube. This hoop reinforcement was adjusted by varying the revolutions of fibre bundle per unit length of the tube. Since NR was compounded in-house, the tube form had to be formed in a laboratory. The process of making the tubular body of an actuator is presented in Fig. 1. In Fig. 1, a tube (length 170 mm, radius 8 mm, inner radius 5 mm) is formed by wrapping a 1.5 mm-thick layer of rubber sheet around a metal rod (diameter 5 mm). The flow of rubber during vulcanization was prevented by wrapping a thin silicone sheet tightly around the tube. The other end of the tube was sealed by a 15 mm-long cap prepared from of the same NR compound. The tube was cured in a heating press at 150°C for 20 minutes. The ends of the commercial tubes (length 170 mm, radius 8 mm, inner radius 5 mm) were sealed by a 1.5 mm-long cap fabricated from acrylic foam

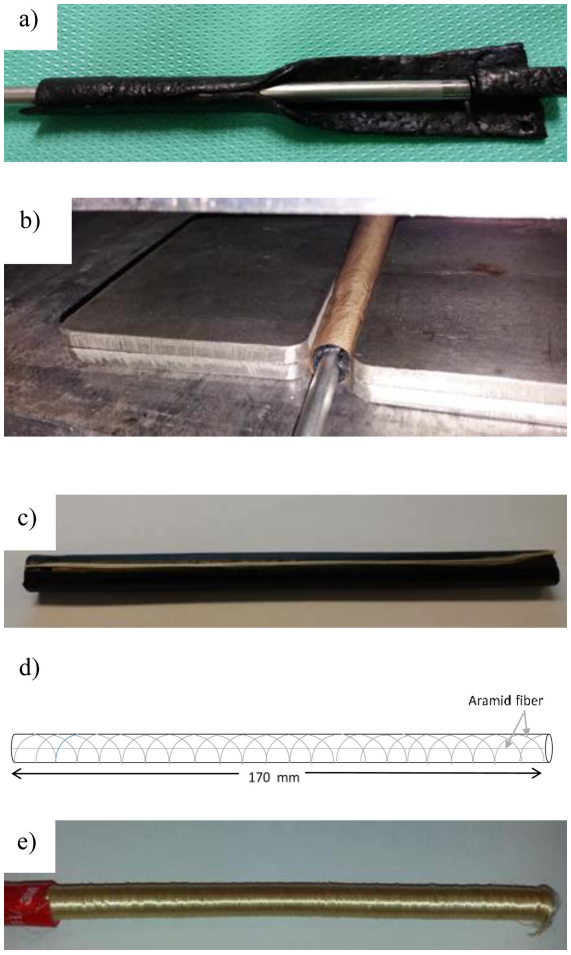

Fig. 1 a)–e) Preparation of fibre-reinforced NR actuator specimens.

film tape (VHB 4910, 3M).

For the fitting process of a numerical material model for elastomer, tensile test specimens were prepared. Tensile specimens were cut from NR sheet with a nominal thickness of 1 mm into a planar, rectangular shape of 110 × 20 mm and standard dog-bone shaped specimens. Due to the hyperelastic nature of elastomers, also biaxial tests were needed for the material model fitting. For biaxial tests, specimens were cut from a NR sheet with a nominal thickness of 1 mm into a planar, rectangular shape of 88 × 88 mm.

3.3 Mechanical testing

Standard tensile tests (dog-bone specimens) were run according to ISO 37 standard. Five NR specimens were tested using a tensile

tester (Messphysik) with a 1 kN load cell and 500 mm/min displacement rate. Additionally, tensile testing (wide specimen) of NR was performed using a tensile tester (Messphysik) with a 1 kN cell. These tests were displacement-controlled, at a constant rate of 10 mm/min, and performed at ambient conditions (30% RH, 26°C); a low displacement rate was used to fit lower strain-range tests with (DIC) measurements in practice as well as the finite element scheme.

Biaxial testing of NR was performed using a biaxial stretcher (KARO IV, Brückner) with a nominal load range 5–200 N, at the premises of VTT Technical Research Centre of Finland. Biaxial tests were displacement-controlled, at a 3/3 stretching ratio, in two subsequent load steps with a dwell time (hold) between load ramps, and at ambient conditions (42% RH, 20.5°C).

The actuation testing of the fibre-reinforced actuators were performed by connecting the actuators to an air pressure source with pressure control, measurement (10 N load cell, LTS-1KA, Kyowa) and analysis software (LabVIEW 2012). The pressure was applied in ≈50 kPa steps (0...500 kPa) to account for any dynamic effects. The load cell was attached to the sealed end and above the actuator specimen.

3.4 Digital image correlation

Strain and displacement fields over the tensile (wide) and biaxial NR specimens were acquired using a two-camera setup and digital image correlation (DIC) analysis software (LaVision). A random speckle pattern was made by using spray paint on one side of tensile and biaxial specimens. Data was synchronized with the testing machines' data by observed first signal peak.

3.5 Optical fibre strain sensing

The actuator internal deformation was traced by using embedded optical fibres with four Fiber Bragg Grating (FBG) sensors multiplexed in each fibre. The signal processing was performed via a W3/1050 Series Fiber Bragg Grating Interrogator (Smart Fibers). A wavelength range of 1510–1590 nm was applied and the interrogator was operated using a Remote Interface W3 WDM (version 1.04). The fibers with the FBGs were individually tailored by Instituto de Telecomunicações (Aveiro, Portugal). Per reinforced actuator, an optical fibre with FBGs was fixed along with the axial aramid fibre reinforcement bundle, under the wound reinforcement layer.

4 Modelling and simulation routines

4.1 Finite element models

Finite element (FE) simulations were performed to (1) fit a hyper-elastic material model and (2) to survey the potential performance of fibre-reinforced elastomeric actuators. All the modelling and implicit solutions were carried out using *Abaqus*® 2017 standard (Simulia). The tensile test specimen (full model, planar dimensions 110 mm × 20 mm, thickness 0.95 mm, Fig. 2) and the bi-axial specimen (quarter model, planar dimensions 44 mm × 44 mm, thickness 1.1 mm, Fig. 3) were modelled to validate a material model for NR. The load was applied as enforced displacement and boundary conditions were given using symmetry and zero displacements at edges. A reinforced actuator was modelled as a system of hyperelastic body and a reinforcement layer covering the body, as shown in Fig. 3. The axial reinforcement was modelled using a partitioned section in the body. All the FE models were meshed using linear C3D8H brick elements (hybrid formulation), see mesh densities in Figs. 2–4.

In order to fit a proper material model for the elastomer body, Abaqus' property fitting tool was used to define parameters for three different hyperelastic models using the standard tensile test data (see Section 3.3). The three material model candidates were second order Ogden, Yeoh, and Neo-Hookean hyperelastic models [11]. The validity of each model was first demonstrated by simulating the tensile test (wide specimen) and subsequently by simulating the biaxial test. For all the hyperelastic material models, NR was the reference material. To compare the simulation

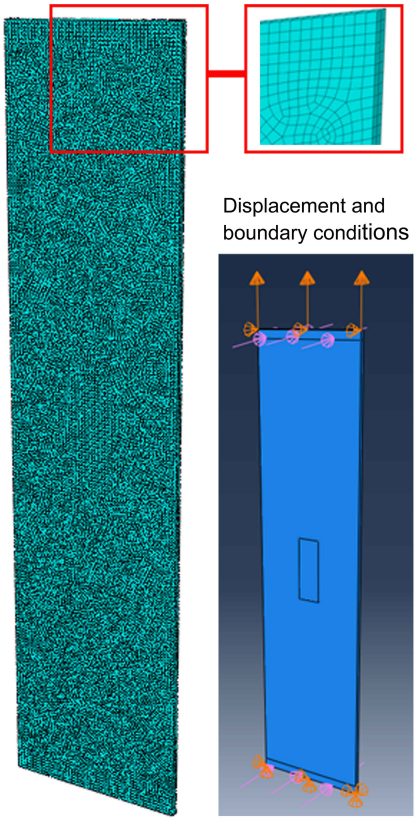

Fig. 2 FE model, element mesh, and boundary conditions of the tensile test specimen.

results with the DIC based strains, data was collected over nodal regions that corresponded to the analysis of the DIC measurements (five points on wide tensile specimen, 60 mm $\times$ 60 mm region on biaxial specimen).

4.2 Actuator performance survey

The performance survey of the reinforced elastomer actuator concept was carried using the process-integration and optimization tool Isight (Simulia). The aim was to understand the criticality of stiffness in different directions in the wound reinforcement. Therefore, the reinforcement layer was modelled by using engineering constants (nine constants in total) of which five were designated as variables (E_{RR}, $E_{\theta\theta}$, E_{ZZ}, Poisson's ratio $\nu_{Z\theta}$). Additionally, the importance of stiffness in the axial reinforcement ($E_{ZZ,axial}$) was included as variable. Latin Hypercube Sampling method was used for defining

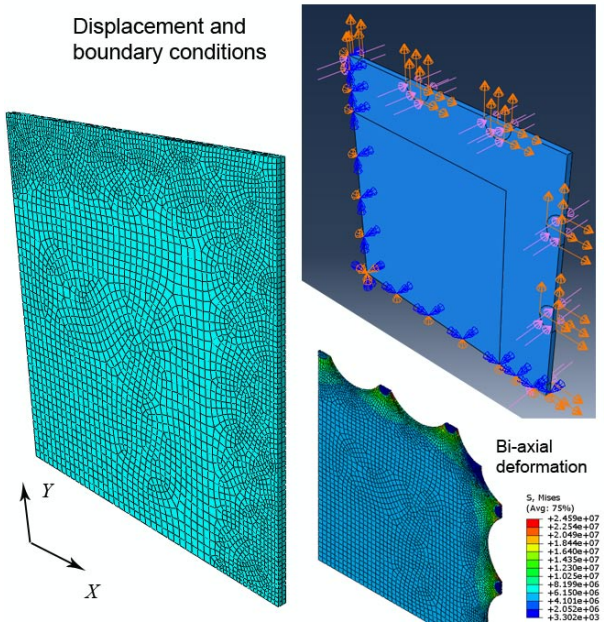

Fig. 3 FE model, element mesh, and boundary conditions of the biaxial test specimen.

the computation case matrix. Here, 50 cases were simulated to estimate the effect of each material parameter over its value range. Finally, the essence of each material parameter was defined using the (linear) Correlation Factor. The target response was the translation (U2) of the actuator free end at the completion of each simulation case. The applied value ranges were as follows:

- E_{RR} : [70 GPa...192 GPa]
- $E_{\theta\theta}$: [70 GPa...192 GPa]

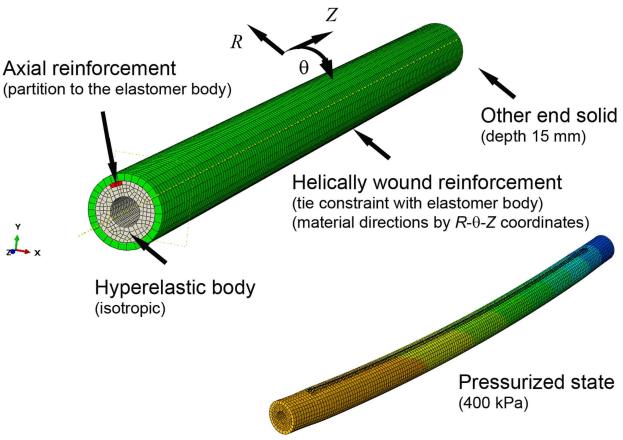

Fig. 4 FE model of the reinforced actuator.

- E_{ZZ} : [0.5 GPa...1.1 GPa]
- $\nu_{Z\theta}$: [0.01...0.33]
- $E_{ZZ,axial}$: [10 GPa...192 GPa]

5 Results and analysis

The ISO-37 tensile test results are shown in Fig. 5. Variation in stiffness between the specimens was low but ultimate strength was scattered due to some air cavities in NR. The results were used to determine the following material model parameters:

- Ogden: μ_1 = 101832.293; α_1 = 3.2073128; μ_2 = 1681595.86; α_2 = -6.5337968; D1 = 4.546361 $\times 10^{-8}$; D2 = 0,
- Yeoh: C10 = 553538.2; C20 = 63425; C3 = -896; D1 = 7.32389 $\times 10^{-8}$; D2 = 0, D3 = 0,
- Neo-Hookean: C10 = 975779.66; D1 = 4.15468186 $\times 10^{-8}$.

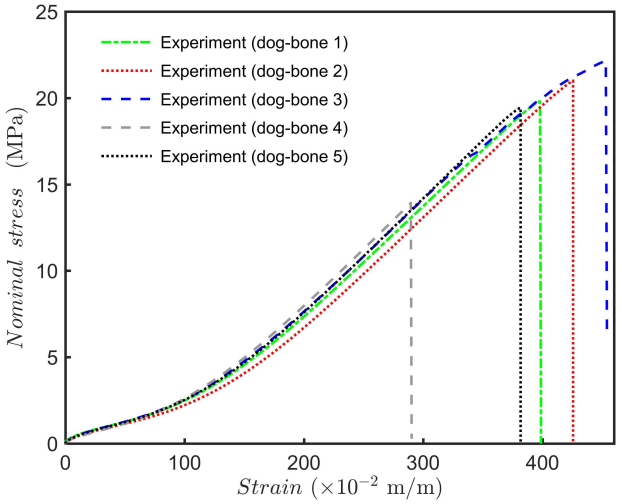

Fig. 5 The standard (dog-bone) tensile test results for NR.

6 Force output results from experiments

The effect of the axial reinforcement type on the force output of a reinforced PDMS actuator is shown in Fig. 6. The results indicate, rather interestingly, that the reinforcement type is not extremely crucial for high force output.

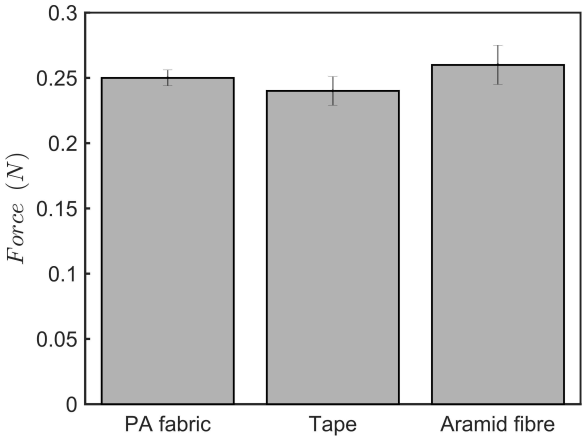

Fig. 6 The effect of axial reinforcement on force output (PDMS actuator body). Applied pressure 500 kPa.

In turn, the effect of the wound hoop reinforcement in terms of the revolutions of bundle wound is clear—the more reinforcement is wound around the tubular elastomer body of an actuator, the higher the capability of the actuator to actuate.

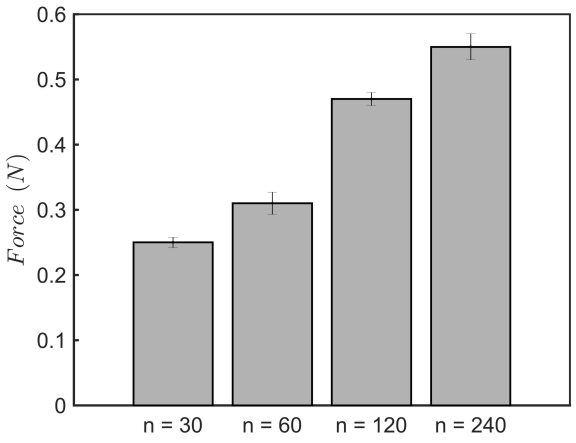

Fig. 7 The effect of wound reinforcement on force output (revolutions of aramid fibre on PDMS body). Applied pressure 500 kPa.

The actuation results in Figs. 6 and 7 showed that the configuration of the wound reinforcement is an essential design item to make a strong elastomer actuator—even more than the axial

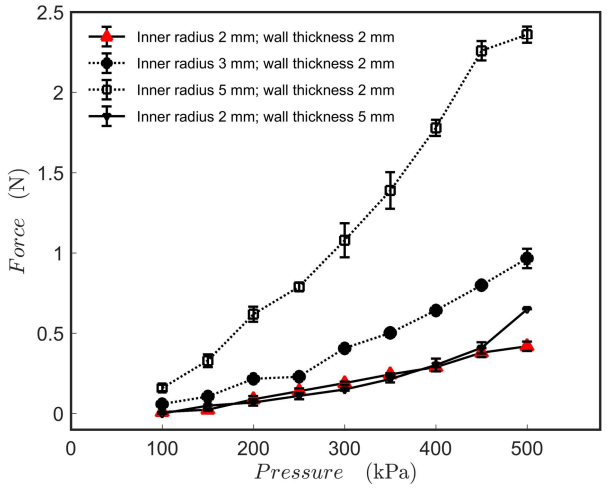

Fig. 8 The effect of tube wall thickness on force output (NR actuator body).

reinforcement underneath the wound reinforcement layer. In addition to the fibrous reinforcement, it is anticipated that the geometry of the tubular body influences the force output. In Fig. 8, it can be seen that the wall thickness of the body affects the force output. As is intuitively clear, a thinner wall will allow the actuator to exert higher forces per given pressure load. Naturally, the wall thickness must be considered with respect to the tube size (outer diameter). Larger tube creates higher absolute force output.

The mass of an elastomeric actuator is mainly determined by the dimensions of the elastomeric body. For example, the PDMS actuators with wound reinforcement (results in Fig. 7) weighed 8.84 g (n=30), 8.75 g (n=60), 8.63 g (n=120), 8.75 g (n=240). The force output lead to weight efficiency values of 28.3, N/kg, 35.4 N/kg, 54.5 N/kg, and 62.9 N/kg, respectively.

6.1 Hyperelastic material model validation

The simulated force-displacement curves for the wide tensile test specimen are shown in Fig. 9. It can be seen that all the three hyperelastic models follow well the experimental reference for low displacement range (say 0–10 mm). For a larger displacement range, the simulated behavior begins to show the character of the standard tests (Fig. 5). To model a reinforced actuator,

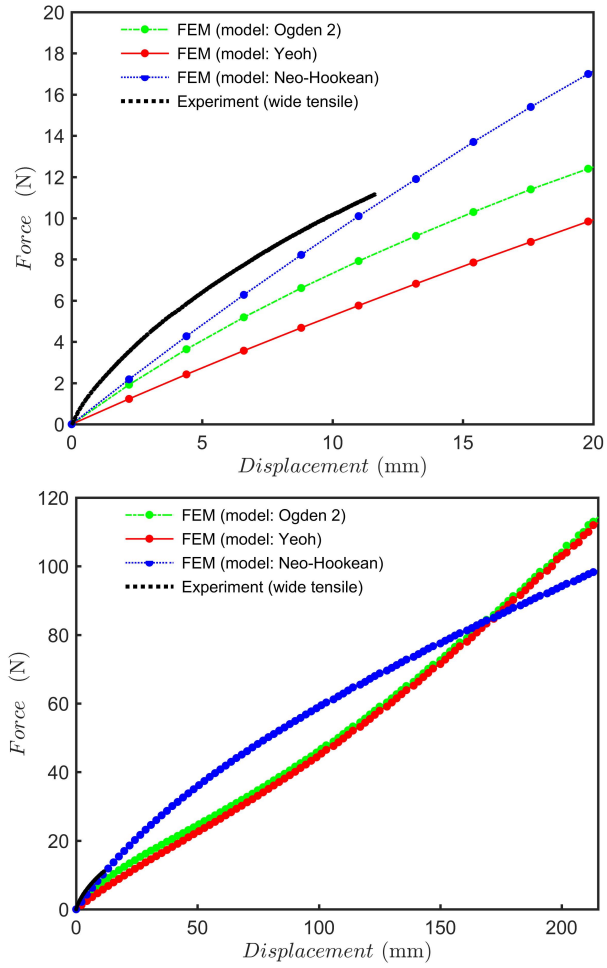

Fig. 9 The simulated tensile test (wide specimen).

model validity over the lower end of displacement (strain) range is important (the test with a wide specimen was run only till 10% strain). The Ogden and Yeoh models produce similar force-displacement curves but the Neo-Hookean behavior is different meaning that the tangent modulus decreases as the displacement (strain) increases. Based on the tensile test simulation, the Neo-Hookean model tends to fit the tensile experiments of this study best.

The simulation results of the biaxial test are shown in Figs. 10 and 11. The simulation and test results are shown separately for the test machine X and Y directions (namely MDX and TDX directions). It can been that the simulated strains (mean value over a central region of 60 mm × 60 mm in the test specimen and 30 mm × 30 mm region in quarter FE model) follow rather

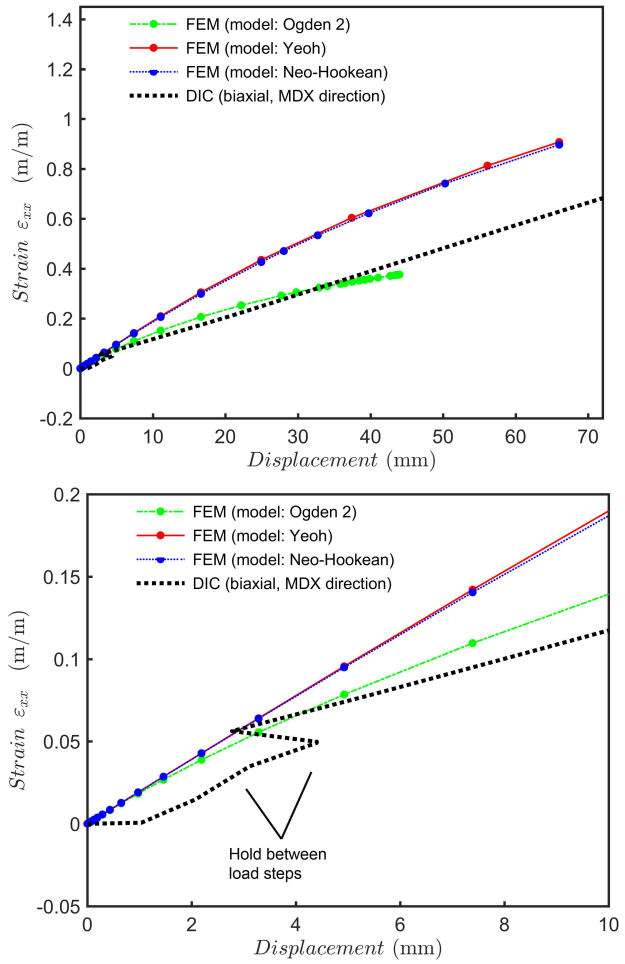

Fig. 10 The simulated biaxial test (MDX direction).

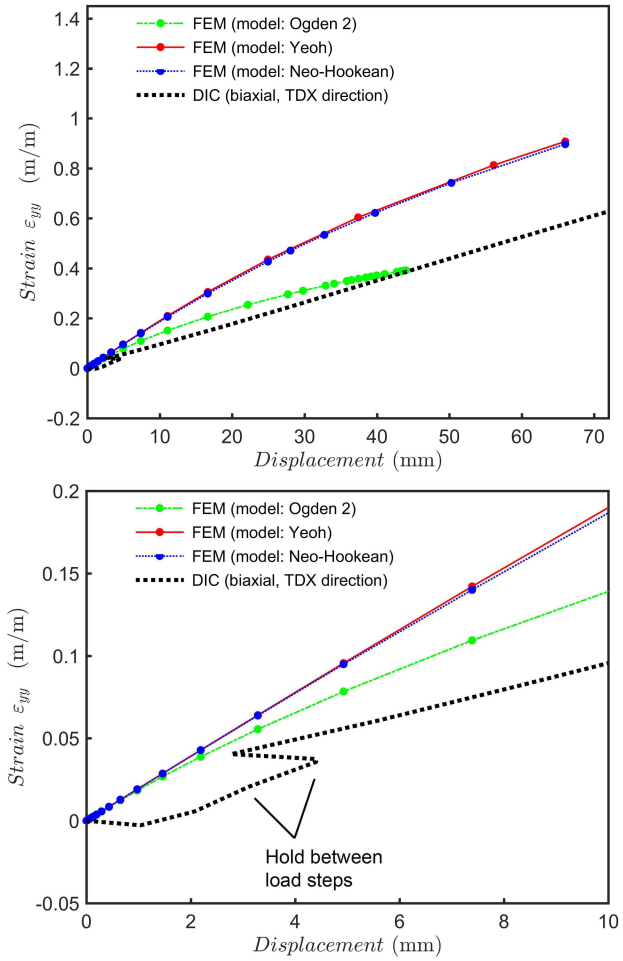

Fig. 11 The simulated biaxial test (TDX direction).

well the experimental results (DIC data from biaxial tests). When comparing the different models, both Yeoh and Neo-Hookean models produce overly loose stretching over the central region of the specimen. In other words, the second order Ogden model concentrates stretching at the test machine gripping region, where the load condition is three-dimensional (pressure of the gripping mechanism was included in the FE model at the specimen edge). Since the strain accumulation predicted by the Ogden model corresponded better the experiment, the fitted Ogden model was selected for the actuator simulation.

6.2 Surveying of essential material properties for actuation performance

The performance of the modelled elastomer actuator was defined as the capability to bend (upwards, in U2 direction). For an unconnected elastomer actuator, the bending performance corresponds to the force output as long as the deformation is stable as a function pressure. The results of the automatized mapping are shown in Fig. 12. Based on the results, it can be seen that the stiffness of the wound reinforcement in the tube's axial direction is of primary importance. Additionally, axial reinforcement underneath the wound reinforcement layer plays a part while the effect of stiffness in the radial and tangential directions is negligible. These results are supported by the experimental results presented in Figs. 6 and 7.

The simulated deformation shape of the reinforced actuator is shown in Fig. 13 demonstrating a correct kind of actuator bending. The FE actuator in this study applied a continuum mod-

el for the wound reinforcement, which is too a stiff compared to the wound aramid fibre bundle in reality. Therefore, the axial deformation is small and the bending results in slight compressive stress state on the actuator surface above the axial reinforcement. When compared to experimental results (FBG strains upon an actuation test are all positive, see Fig. 14), the real actuator is essentially free to deform (stretches) axially because the wound reinforcement layer does not create a stiffening effect in the axial direction.

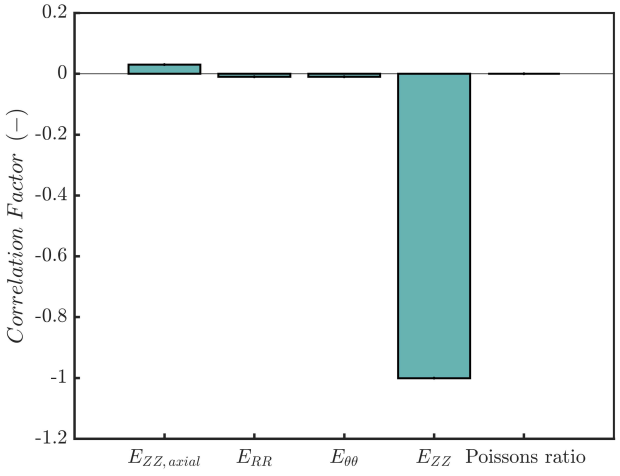

Fig. 12 The automated simulation routine results.

6.3 Conclusions

This study includes three different parts: (1) a literature survey of the efficiency of various types

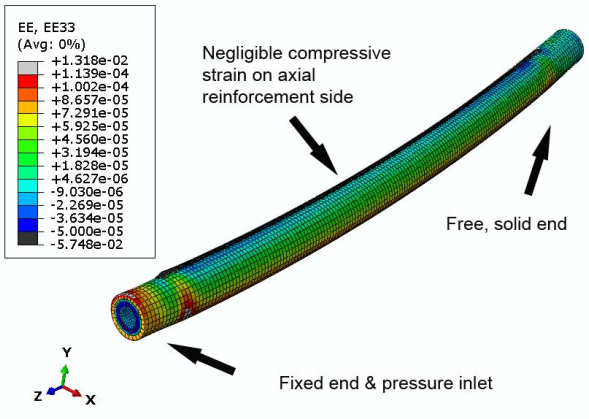

Fig. 13 Simulated behavior of the fibre-reinforced elastomer actuator.

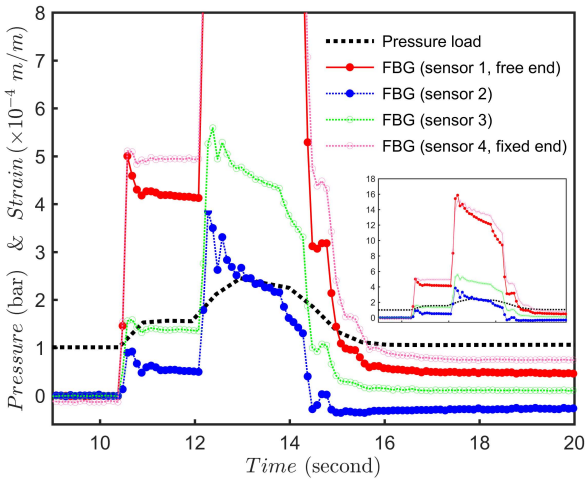

Fig. 14 Load-strain results using FBG sensors embedded into the actuator.

of actuators in airborne vehicles, (2) an experimental work entity to study elastomeric fibre-reinforced actuators, and (3) a numerical simulation entity to survey the essential material parameters when developing an efficient elastomer actuator. Based on the results, the weight-normalized force output of soft actuators is nowadays low and further research is needed to profit the advantage of soft actuators in aircraft applications. Our experimental results show that a tubular elastomer actuator can be made anisotropic to produce moments. The bending actuation requires efficient reinforcement in the axial direction both for controlling the *local* stiffness along the long axis of the actuator and to reinforce the elastic walls against a high internal pressure. The weight efficiency of the laboratory scale actuators was 28–63 N/kg, which is in the order of weight efficiency of electro-mechanical servo actuators in model planes and UAVs. Based on the FE simulations in this study, the wound reinforcement concept, a low helical angle, i.e. low axial stiffness, is of primary importance to produce extensive bending actuation.

6.4 Acknowledgements

This study was funded by a grant from Academy of Finland (project ActiveFit). The authors want to acknowledge researcher Olli Orell (Tampere University of Technology, Finland) for

DIC measurements, Satu Pasanen for biaxial testing (VTT, Finland), and researcher Jarno Jokinen (Tampere University of Technology, Finland) for support in the simulation work. Professor Jyrki Vuorinen and Professor Reza Ghabcheloo (Tampere University of Technology, Finland) are acknowledged for their project-organizational actions.

References

[1] Polygerinos P, Wang Z and Overvelde JTB. Modeling of soft fiber-reinforced bending actuators. *IEEE Transactions on Robotics*, Vol. 31, No. 3, pp 778–789, 2015.

[2] Galloway KC, Polygerinos P, Walsh CJ and Wood RJ. Mechanically programmable bend radius for fiber-reinforced soft actuators. *16th International Conference on Advanced Robotics 2013 (Proceedings)*, Montevideo, Uruguay, November 25-29, pp 1-6, 2013.

[3] Kanerva M, Poikelispää M and Vuorinen J. Continuum simulation of hyper-elastic elastomer actuators: the effect of material models. *Molecular order and mobility in polymer systems - 9th International IUPAC Symposium (Book of Abstracts)*, St.Petersburg, Russia, June 19-23, O-91, pp 115–116, 2017.

[4] Technical specifications. *Aerospace Actuators*. Parker, http://ph.parker.com/us/, 2018 (cited).

[5] Product description. *MiniAct Magnetic Actuator*. Plantraco, http://microflight.com/, 2018 (cited).

[6] Shintake J, Rosset S, Schubert BE, Floreano D, Shea HR. A Foldable Antagonistic Actuator. *IEEE/ASME Transactions on Mechatronics*, Vol. 20, No. 5, pp 1997–2008, 2015.

[7] Technical data sheet. *Actuators, Air bellows*. IMI Norgren, http://pages/norgren.com/, 2018 (cited).

[8] Technical data sheet. *Fluidic Muscle*. Festo, https://www.festo.com/, 2017/10).

[9] Design information. *PneuNets Bending Actuators*. Soft Robotics Toolkit, http://softroboticstoolkit.com/, 2018 (cited).

[10] Gorissen B, Chishiro T, Shimomura S, Reynaerts D, and De M. et al. Flexible pneumatic twisting actuators and their application to tilting micromirrors. *Sensors Actuators A Phys*, Vol. 216, pp 426–431, 2014.

[11] Ali A, Hosseini M, Sahari BB. A Review of constitutive models for rubber-like materials. *American Journal of Engineering and Applied Sciences*, Vol. 3, No. 1, pp 232–239, 2010.

7 Contact Author Email Address

mailto: Mikko.Kanerva@tut.fi

Copyright Statement